

Supplementary Information

Interfacial Regulation via Configuration Screening of Disodium Naphthalenedisulfonate Additive Enabled High-Performance Wide-pH Zn-based Batteries†

Hui Lin,^a Lingxing Zeng,^{*ac} Chuyuan Lin,^a Junxiu Wu,^{*b} Huibing He,^d Chengxiu Huang,^a Wenbin Lai,^a Peixun Xiong,^d Fuyu Xiao,^a Qingrong Qian,^{ac} Qinghua Chen^{ac} and Jun Lu^{*b}

^a Engineering Research Center of Polymer Green Recycling of Ministry of Education, Fujian Key Laboratory of Pollution Control & Resource Reuse, College of Environmental and Resources, Fujian Normal University, Fuzhou, Fujian 350007, China. E-mail: zenglingxing@fjnu.edu.cn

^b College of Chemical and Biological Engineering, Zhejiang University, Hangzhou, Zhejiang 310027, China. E-mail: wujunxiu@zju.edu.cn; junzoelu@zju.edu.cn

^c Key Laboratory of Advanced Energy Materials Chemistry (Ministry of Education), College of Chemistry, Nankai University, Tianjin 300071, China.

^d School of Chemistry and Chemical Engineering, Guangxi Key Laboratory of Electrochemical Energy Materials, Guangxi University, Nanning 530004, China

^e Inorganic Chemistry I, Technische Universität Dresden, Bergstrasse 66, 01069 Dresden, Germany

Keywords: zinc-metal batteries, electrolyte additive, molecular layer, wide-pH range

Experimental Section

Materials

The zinc sulfate heptahydrate ($\text{ZnSO}_4 \cdot 7\text{H}_2\text{O}$, AR, 99%), potassium hydroxide (KOH, AR, $\geq 85.0\%$), sodium sulfate anhydrous (Na_2SO_4 , AR, 99%) and manganese sulfate monohydrate ($\text{MnSO}_4 \cdot \text{H}_2\text{O}$, AR, 99%) were provided by Aladdin. Naphthalenedisulfonic acid disodium salt ($\text{C}_{10}\text{H}_6\text{Na}_2\text{O}_6\text{S}_2$), e.g., 15 NADS, 16 NADS, 26 NADS, and 27 NADS, was purchased from Macklin. Zn foil (99.98% purity, thickness 0.25 mm) was purchased from the Alfa Aesar. The Zn foil used for depth of discharge (DOD) was manufactured by grinding zinc sheets to a thickness of 0.07 mm by roll milling. The Ti foil and active carbon (AC) were procured from the Cyber Electrochemical Materials Network. The glass fibre separators were supplied by Whatman (GF/A or GF/D). $\text{Ni}_{0.8}\text{Co}_{0.1}\text{Mn}_{0.1}\text{O}_2$ powder was obtained from Shenzhen Huaqing New Material Technology Co., Ltd. 1-methyl-2-pyrrolidone (NMP, AR, $\geq 99.0\%$), polyvinylidene difluoride (PVDF, average Mw ~ 534000 , powder), and carbon Super P (SP) were purchased from Sinopharm Chemical Reagent Co. Ltd.

Preparation of Electrolytes and Batteries

ZnSO_4 (2.904 g, 2 mol) and different concentrations of NADS were dissolved in deionised water (5 mL) to form the acidic electrolytes. KOH (0.28 g, 1 mol) and NADS (0.00025 g, 1.5 mmol) were dissolved in deionised water (5 mL) as the alkaline electrolytes. Activated carbon, PVDF, and SP were weighed at a ratio of 8:1:1, and a certain amount of NMP was added for grinding; the mixture was then coated on a Ti foil as a positive electrode for the capacitors. The MnO_2 was prepared as the positive

electrode for a full battery using electrodeposition. NCM811, PVDF, and SP were weighed at 8:1:1 and a certain amount of NMP was added for grinding, and the mixture was splashed onto a carbon cloth as a positive electrode to assemble alkaline full batteries.

An acidic Zn||Zn symmetrical batteries were assembled into coin battery (CR2032-type) with Zn foil as the anode/cathode, 2 M ZnSO₄ and 2 M ZnSO₄-26 NADS aqueous solutions as the electrolyte, and glass fibre (Whatman GF/A) as the separator. The Zn||MnO₂ full battery was fabricated in a coin battery using Zn foil as the anode, MnO₂/carbon cloth electrode as the cathode, 2 M ZnSO₄-0.2 M MnSO₄ aqueous solution and 2 M ZnSO₄-26 NADS-0.2 M MnSO₄ as the electrolyte, and glass fibre (Whatman GF/A) as the separator. A Zn powder||MnO₂ full battery was fabricated in a coin battery using Zn powder as the anode, a MnO₂/carbon cloth electrode as the cathode, 2 M ZnSO₄-0.2 M MnSO₄-26 NADS aqueous solution as the electrolyte, and glass fibre (Whatman GF/A) as the separator. The Zn||AC capacitor was assembled with Zn foil as the anode/cathode, 2 M ZnSO₄-26 NADS aqueous solution as the electrolyte and glass fibre (Whatman GF/A) as the separator. The 190 mAh of Zn || MnO₂ pouch cell (10 × 11 cm²) was fabricated using Zn foil as the anode (9 × 9 cm²) and the high mass loading of MnO₂ (25 mg cm⁻², 8 × 8 cm²) as cathode, 2 M ZnSO₄-0.2 M MnSO₄-26 NADS aqueous solution as the electrolyte, and glass fiber (Whatman GF/A) as the separator. For the dilute electrolyte, the Zn||Zn symmetrical battery and Zn||MnO₂ full battery were assembled to coin-type batteries, the 0.3 M ZnSO₄-26 NADS aqueous solution as electrolyte and glass fibre (Whatman GF/A) as the separator. The alkaline

Zn||Zn symmetrical batteries were assembled into coin batteries with Zn foil as the anode/cathode, 1 M KOH-26 NADS aqueous solutions as the electrolyte and glass fibre (Whatman GF/D) as the separator. The Zn||Ni_{0.8}Co_{0.1}Mn_{0.1}O₂ battery was assembled into a coin battery using Zn foil as the anode, Ni_{0.8}Co_{0.1}Mn_{0.1}O₂ as the cathode, a 1 M KOH-26 NADS aqueous solution as the electrolyte, and glass fibre (Whatman GF/D) as the separator.

Electrochemical Measurements

Tafel, linear sweep voltammetry (LSV), and cyclic voltammetry (CV) curves were obtained using a three-electrode system (reference electrode, Ag/AgCl) at a scan rate of 5 mV s⁻¹. The chronoamperometry (CA) transient curves were tested at -150 mV. The above experiments were undertaken in ZnSO₄/ZnSO₄-26 NADS electrolytes.

CV test yields nucleation overpotential (NOP), and the r_{crit} and NOP have the following relationship:

$$r_{crit} = 2 \frac{\gamma V_m}{F|\eta|} \quad (S1)$$

Where γ and V_m are the surface energy and molar volume of the Zn anode, respectively, F is the Faraday constant and η is the NOP.

The relationship between the nucleation rate ω and the NOP of Zn is as follows

$$\omega = K \exp\left(\frac{\pi h \sigma^2 L A}{\rho n F R T \eta}\right) \quad (S2)$$

where K is the pre-exponential factor, n is the valence number of metal ions ($n = 2$ for Zn²⁺ ions), σ is the interfacial tension, L is the Avogadro number, R and F are the gas constant and Faraday constant, T is the absolute temperature, ρ , A and h are the density, atomic weight and atomic height of the deposited metal Zn, respectively.

Electrochemical impedance spectroscopy (EIS) was measured at a sinusoidal perturbation of 5 mV and in the frequency range of 0.1 Hz ~ 100 kHz. The differential capacitance curve was calculated from the equation (S3):

$$C = \frac{1}{2\pi f Z_{im}} \quad (S3)$$

where C is the differential capacitance, f is the frequency, Z_{im} is the imaginary part of the impedance, and a specific frequency of 1000 Hz.

Electrochemical characterisation tests were conducted using an Ivium-N-stat.

Computational Methods

Density functional theory (DFT) computations were performed using the Vienna ab initio simulation package (VASP) using the projector augmented wave (PAW) method.^[S1-3] The exchange correlation potential was represented by the Perdew–Burke–Ernzerhof (PBE) functional within the generalised gradient approximation (GGA).^[S4] ESP calculations were conducted using the GaussView package in the Gaussian (G09) program. The B3LYP functional was adopted for all calculations in combination with the D3BJ dispersion correction.^[S5,6] In geometry optimization and frequency calculations, the 6-311G(d,p) basis set was used.^[S7] The frontier molecular orbital and electrostatic potential (ESP) figures were drawn by Multiwfn.^[S8]

The MD simulations were performed in the GROMACS 2021 software package.^[S9-S11] In the ZS electrolyte, the monomer ratio of ZnSO₄: H₂O = 2:55.56 and 200 ZnSO₄, 5556 water molecules were randomly inserted into a cube box with a side length of 6.0 nm. In the ZS-26 NADS electrolyte, the monomer ratio of ZnSO₄: H₂O: 26 NADS = 2: 55.56: 0.2, 200 ZnSO₄, 5556 water and 20 26 NADS molecules were

randomly inserted into a cube box with a side length of 6.0 nm.

Then, a 6×6×1 superbattery Zn (002) surface with five atomic layers was fabricated. The thickness along c direction of Zn(002) was set at 35 Å. During the optimisation process, the bottom two layers of atoms were fixed and the top three layers of atoms were relaxed. The cutoff energy was set to 450 eV and the k-point sampling grid was set to 1×1×1. The self-consistent calculations applied a convergence energy threshold of 10⁻⁵ eV. Additionally, the adsorption energy (E_{ad}) of H₂O, four NA²⁻ ions on the Zn (002) surface was calculated as follows:

$$E_{ad} = E_{(Zn+adsorbate)} - E_{(Zn)} - E_{(adsorbate)}$$

where $E_{(Zn + adsorbate)}$, $E_{(Zn)}$ and $E_{(adsorbate)}$ are the total energies of the Zn (002) surface with the adsorbate and the Zn (002) surface and adsorbate, respectively.

The COMSOL used a cubic current distribution physical field simulation where the fluxes of the substances were calculated by the Nernst-Planck equation:

$$N_i = -D_i \nabla c_i - z_i u_i F c_i \nabla \varphi_1$$

where N_i , c_i , z_i , u_i , F , φ_1 denotes the transfer vector ($\text{mol m}^{-2} \text{s}^{-1}$), the concentration in the electrolyte (mol m^{-3}), the charge of the ionic substance, the mobility of the charged substance ($\text{m}^2 \text{V}^{-1} \text{s}^{-1}$), denotes Faraday's constant (As mole^{-1}), and denotes the potential in the electrolyte (V), respectively. i denotes the different substance. The model size is 50*200 μm , the upper boundary is set to 0.2 V for the cathode and the lower boundary is set to 0 V for the anode. The applied current density is 4 mA cm^{-2} .

Other Characterizations

X-ray diffraction (XRD) was performed on a Bruker D8 diffractometer using

filtered Cu-K α radiation under 40 kV and 20 mA. The microstructures of the as-prepared samples were investigated using scanning electron microscopy (SEM) (Hitachi 8010). Fourier transform infrared (FTIR) spectra were recorded using a Bruker Vertex 70 spectrometer. Atomic force microscopy (AFM) was performed using Nano Wizard 4. Raman spectroscopy experiments were performed using A Horiba LabRAM HR Evolution instrument. The contact angle was measured using Dataphysics Oca 15ec. In-situ microscopic was performed using a Nikon C-PSN microscope.

The Ea was fitted by the equation (S4):

$$\frac{1}{R_{ct}} = A \exp\left(-\frac{E_a}{RT}\right) \quad (\text{S4})$$

where A, R, Ea, and T represent the pre-exponential factor, molar gas constant, activation energy, and absolute temperature respectively.

Table S1. Fitting of corrosion voltage (E_{corr}) and corrosion current (I_{corr}) from Tafel measurements of a series NADS.

Product name	ZS	ZS-15 NADS	ZS-16 NADA	ZS-26 NADS	ZS-27 NADS
E_{corr} (V)	-0.976	-0.969	-0.975	-0.967	-0.973
I_{corr} (mA cm ⁻²)	1.12	0.92	1.01	0.89	0.94

Table S2. The HER overpotentials of a series of NADS isomers at the current density of 10 mA cm⁻².

Product name	ZS	ZS-15 NADS	ZS-16 NADA	ZS-26 NADS	ZS-27 NADS
HER overpotential (V)	-1.07	-1.13	-1.11	-1.22	-1.11

Table S3. The average key lengths of O adsorbed on the Zn (002) plane of a series of NADS isomers.

Product name	15 NA²⁻	16 NA²⁻	26 NA²⁻	27 NA²⁻
Average bond length (Å)	2.16	2.15	2.13	2.20

Table S4. The costs of a series of NADS isomers.

Product name	15 NADS	16 NADS	26 NADS	27 NADS
Cost (USD kg ⁻¹)	182.56	292.09	155.17	282.96

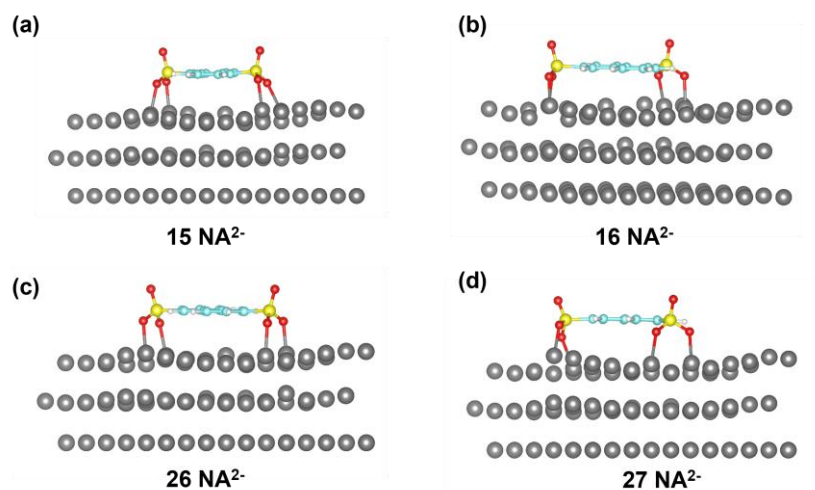


Fig. S1. The pictures of absorption of (a) 15 NA^{2-} ; (b) 16 NA^{2-} ; (c) 26 NA^{2-} ; (d) 27 NA^{2-} .

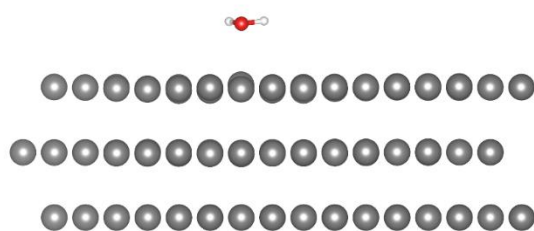


Fig. S2. The picture of absorption of H_2O .

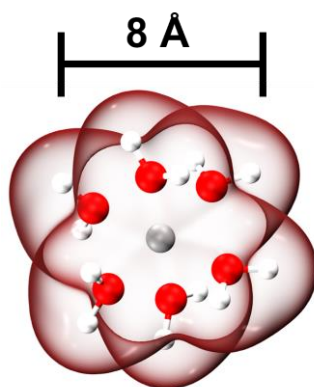


Fig. S3. The ESP and sizes of the $[\text{Zn}(\text{H}_2\text{O})_6]^{2+}$.

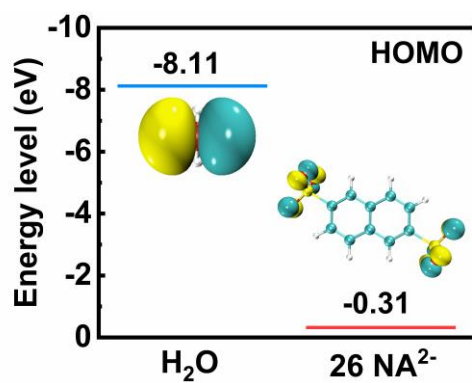


Fig. S4. The DFT calculation results of the HOMO energy level of H₂O and 26 NA²⁻.

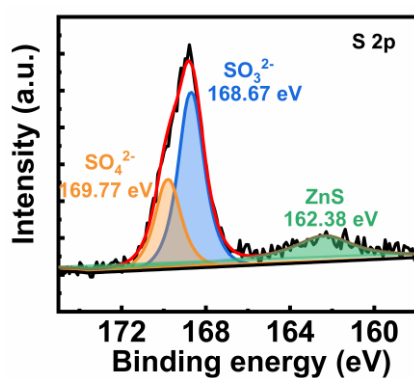


Fig. S5. XPS spectrum of S 2p on Zn foil after cycling in ZS-26 NADS electrolyte.

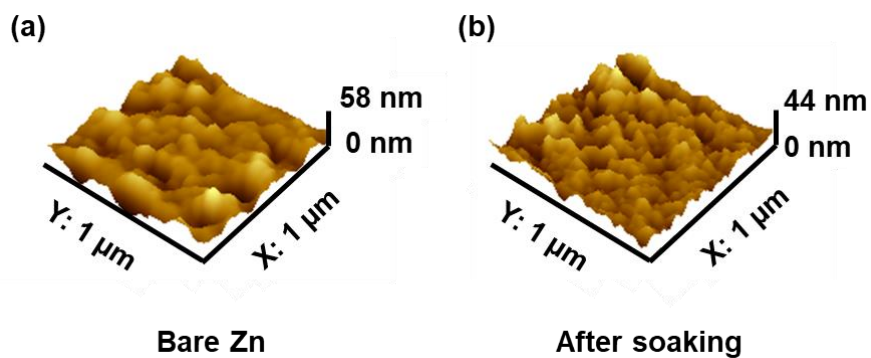


Fig. S6. The AFM results of bare Zn and the Zn foils after soaking in the ZS-26 NADS electrolyte.

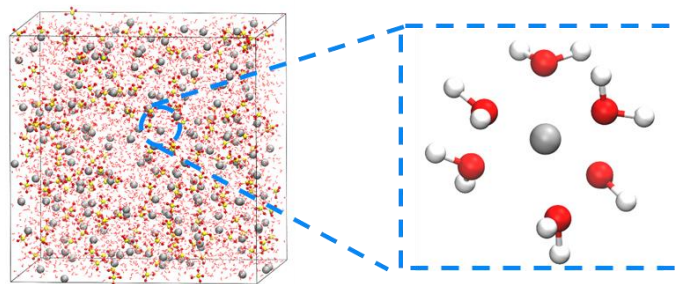


Fig. S7. Snapshots of the MD simulation cells and representative solvation structure in the ZS electrolyte.

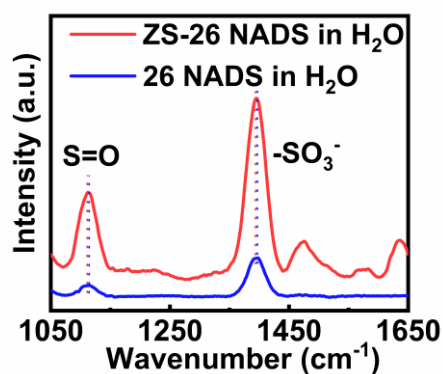


Fig. S8. The Raman spectrograms of 26 NADS/ZS-26 NADS in H₂O.

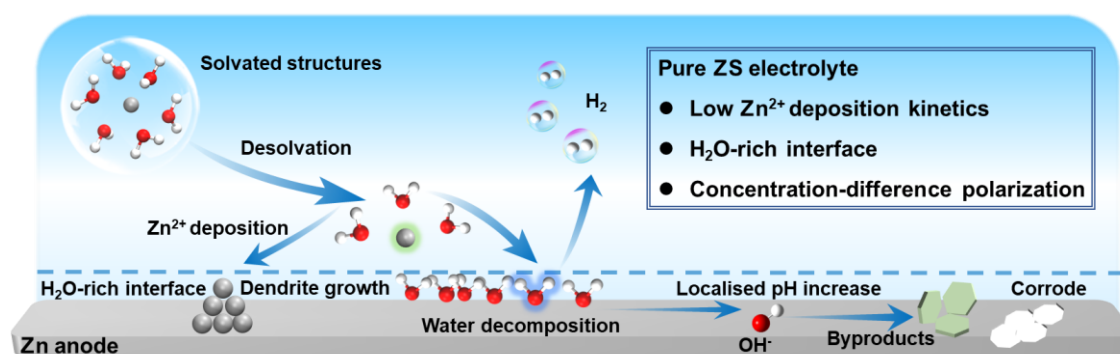


Fig. S9. The Schematic of Zn anode in ZS electrolyte.

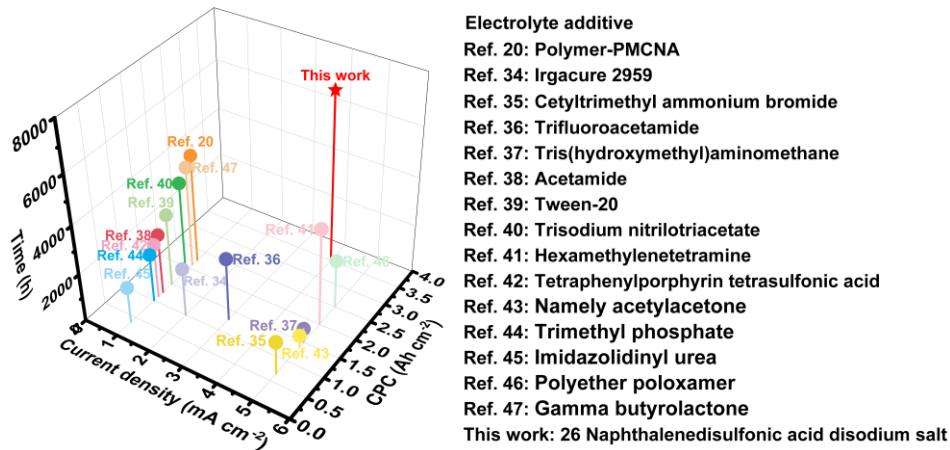


Fig. S10. This work compares the cumulative plating capacity, time and current density with recent related reports.

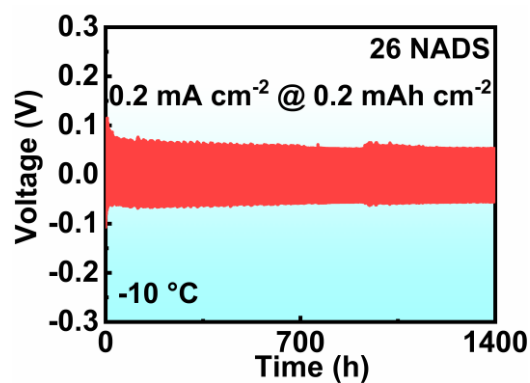


Fig. S11. Cycling performance of Zn||Zn symmetrical battery in the ZS-26 NADS electrolyte at 0.2 mA cm^{-2} @ 0.2 mAh cm^{-2} in the temperature of $-10 \text{ }^\circ\text{C}$.

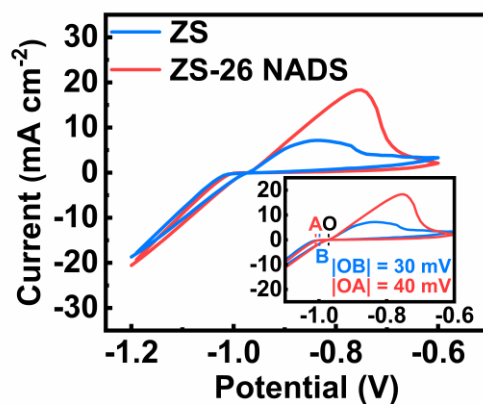


Fig. S12. CV curves at a scan rate of 5 mV s^{-1} in ZS/ZS-26 NADS electrolytes.

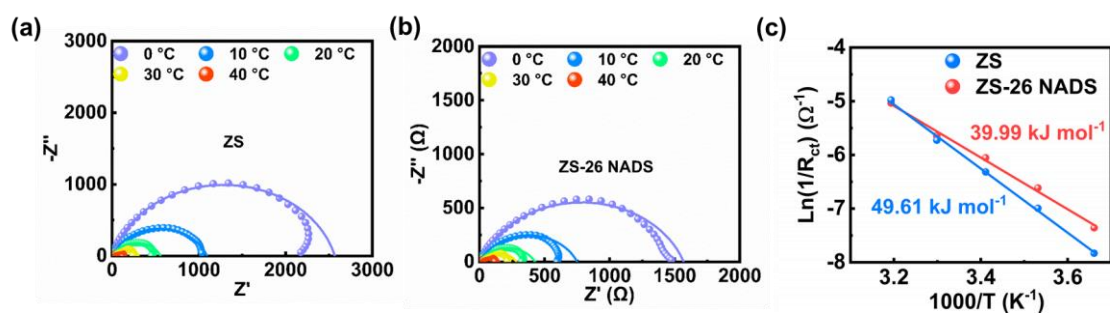


Fig. S13. The EIS results of Zn symmetric batteries at different temperatures in (a) ZS electrolyte and (b) ZS-26 NADS electrolyte. (c) The activation energy of Zn^{2+} depositions in the ZS/ZS-26 NADS electrolytes.

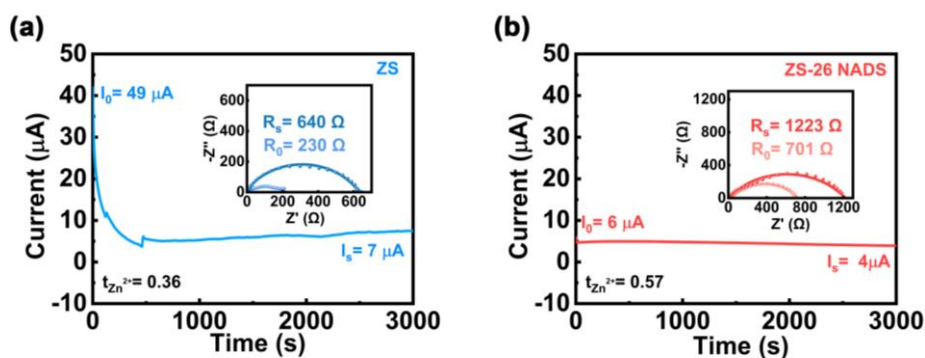


Fig. S14. The transport numbers of Zn^{2+} in (a) ZS electrolyte and (b) ZS-26 NADS electrolyte.

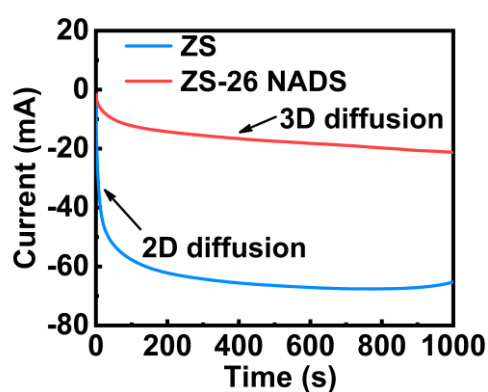


Fig. S15. Measurements chronoamperometry transient curves of ZS/ZS-26 NADS electrolytes.

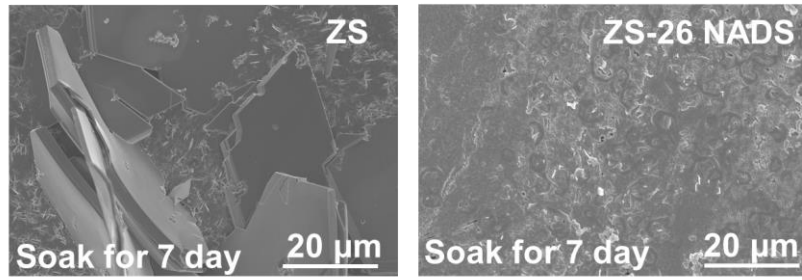


Fig. S16. The SEM images of Zn foils after soaking in the ZS/ZS-26 NADS electrolytes.

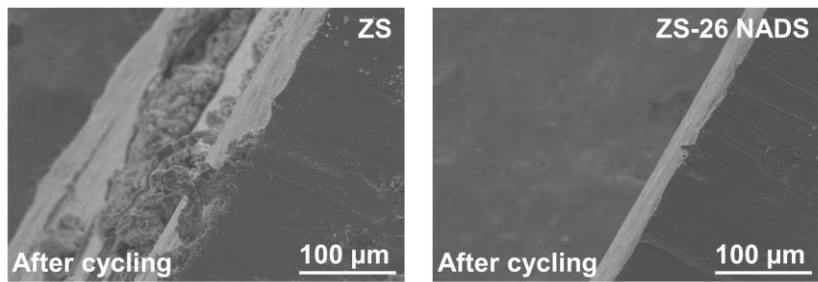


Fig. S17. The SEM images of Zn anodes after cycling at cross-section in the ZS/ZS-26 NADS electrolytes.

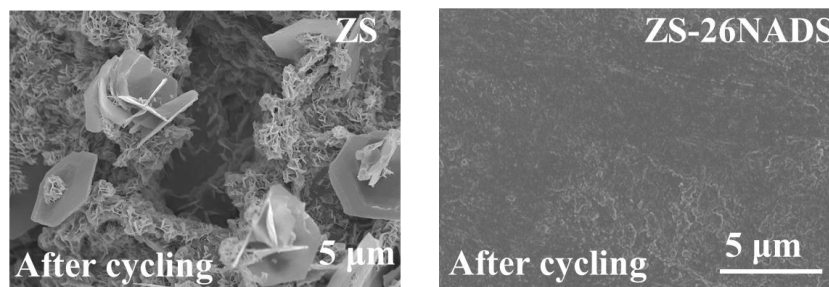


Fig. S18. The SEM images of Zn anodes after cycling in the ZS/ZS-26 NADS electrolytes at a flat.

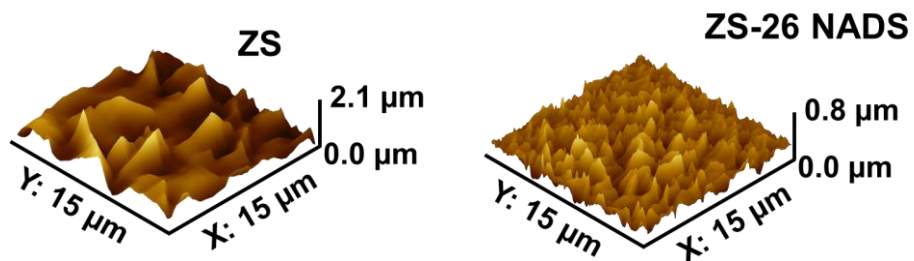


Fig. S19. The AFM results of Zn foils after 30 cycles at 5@2 in ZS/ZS-26 NADS electrolytes.

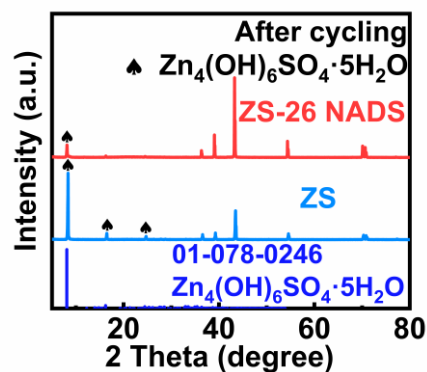


Fig. S20. The XRD patterns of Zn foils after cycling in ZS/ZS-26 NADS electrolytes.

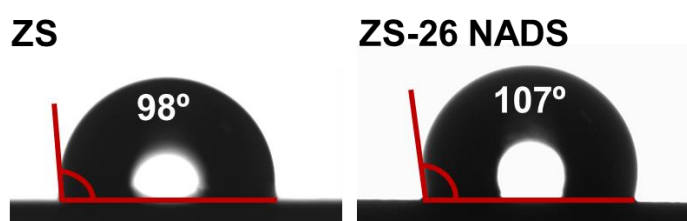


Fig. S21. Contact angle measurement results on Zn foils in ZS/ZS-26 NADS electrolytes.

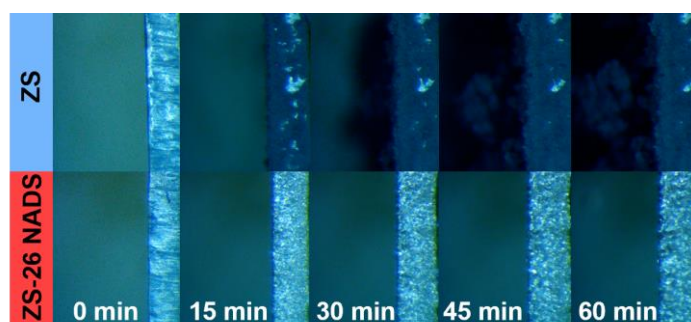


Fig. S22. In-situ microscopy tests of Zn electrodes cycling at 5@5 in ZS/ZS-26 NADS electrolytes.

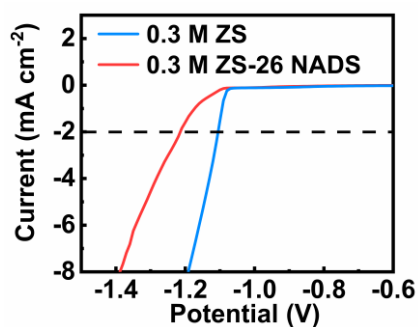


Fig. S23. The linear sweep voltammetry curves (LSV) in 0.3 M ZS/0.3 M ZS-26 NADS electrolytes.

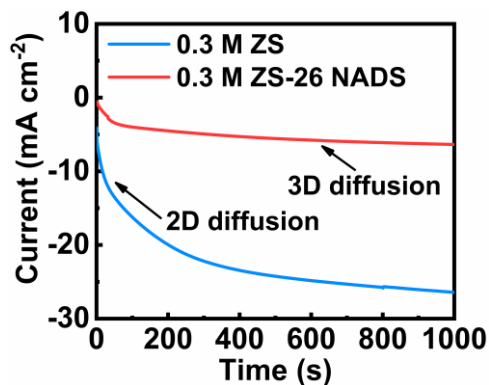


Fig. S24. Measurements of chronoamperometry transient curves of 0.3 M ZS/0.3 M ZS-26 NADS electrolytes.

(a) KOH electrolyte



(b) KOH-26 NADS electrolyte

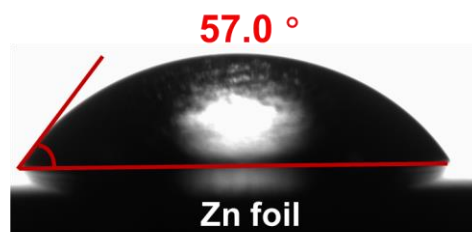


Fig. S25. Contact angle measurement results of the KOH/KOH-26 NADS electrolytes on Zn foils.

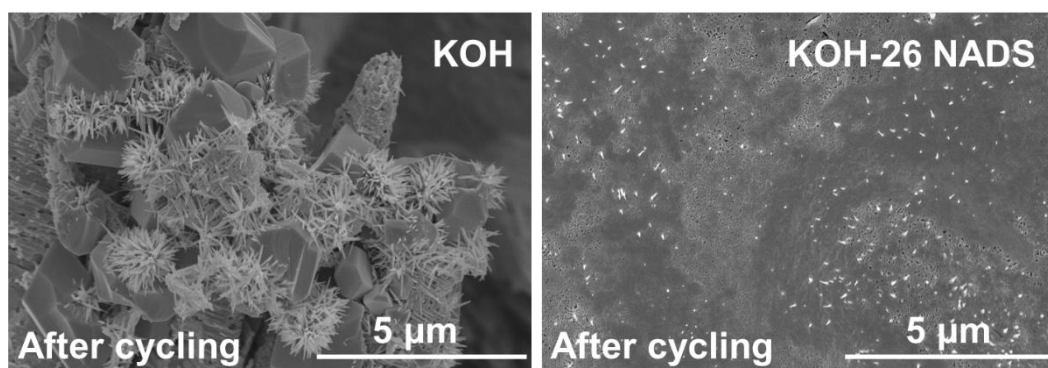


Fig. S26. The SEM images of Zn anodes for Zn||Zn symmetrical batteries in the KOH/KOH-26 NADS electrolytes after cycling.

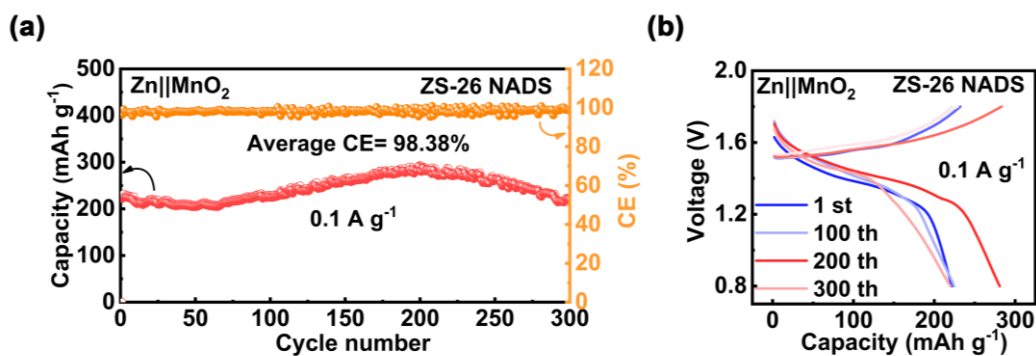


Fig. S27. (a) The cycling performance, Coulombic efficiency and (b) charge/discharge curves of Zn||MnO₂ full battery in the ZS-26 NADS electrolyte with 0.2 M MnSO₄ at 0.1 A g⁻¹.

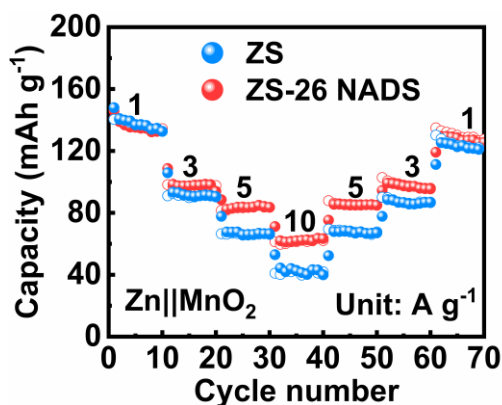


Fig. S28. Rate performances of Zn||MnO₂ full batteries in the ZS/ZS-26 NADS electrolytes.

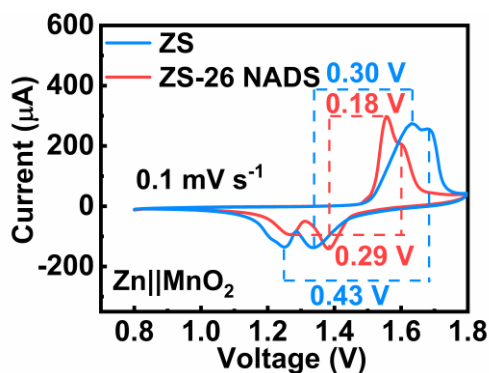


Fig. S29. CV curves of Zn||MnO₂ batteries in the ZS/ZS-26 NADS electrolytes at a scan rate of 0.1 mV s⁻¹.

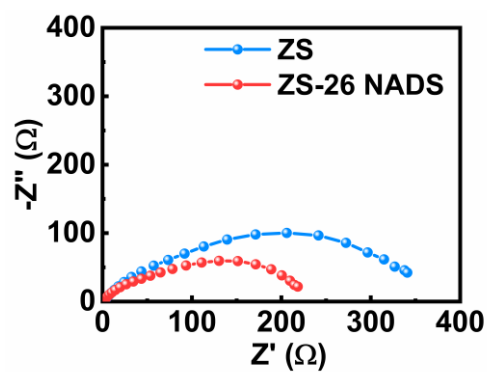


Fig. S30. The EIS results of initial Zn||MnO₂ full batteries in the ZS/ZS-26 NADS electrolytes.

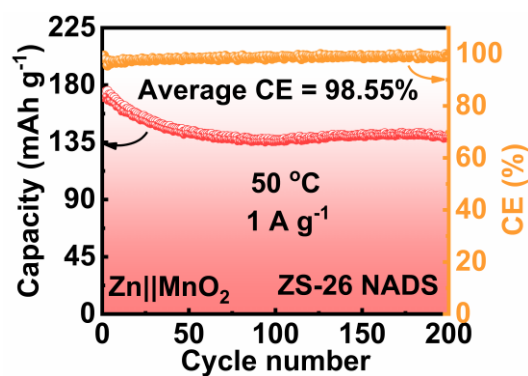


Fig. S31. The cycling performance and Coulombic efficiency of Zn||MnO₂ full battery in the ZS-26 NADS electrolyte at 50 °C.

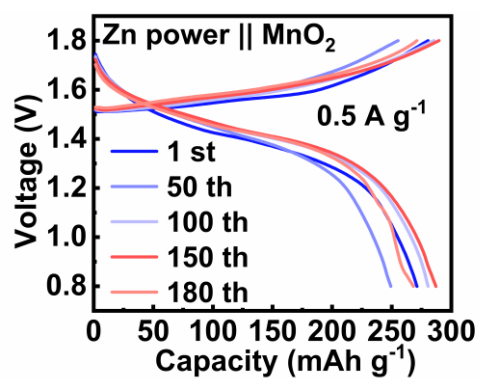


Fig. S32. The charge/discharge curves of Zn power||MnO₂ full battery in the ZS-26 NADS electrolyte at 0.5 A g⁻¹.

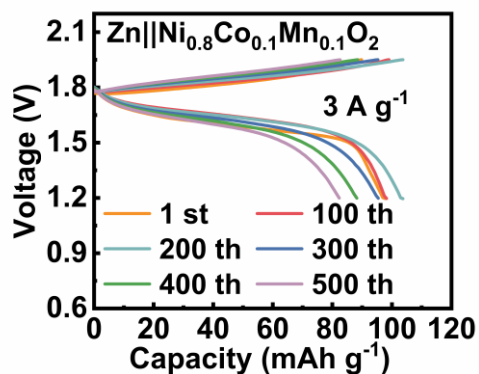


Fig. S33. The charge/discharge curves of Zn||Ni_{0.8}Co_{0.1}Mn_{0.1}O₂ full battery in the KOH-26 NADS electrolyte at 3 A g⁻¹.

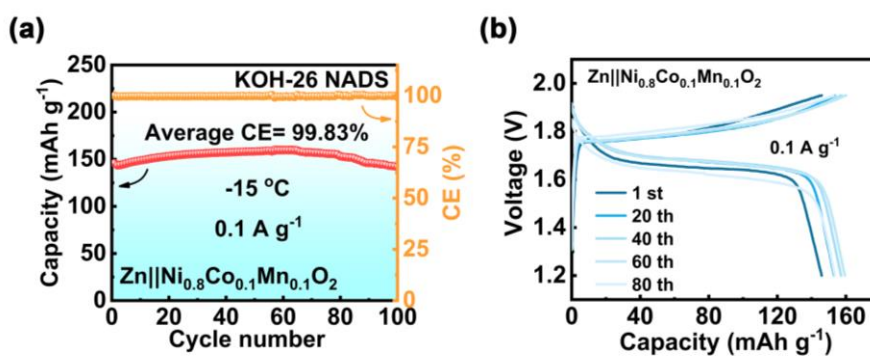


Fig. S34. (a) The cycling performance, Coulombic efficiency and (b) charge/discharge curves of Zn||Ni_{0.8}Co_{0.1}Mn_{0.1}O₂ full battery in the KOH-26 NADS electrolyte at 0.1 A g⁻¹ at -15 °C.

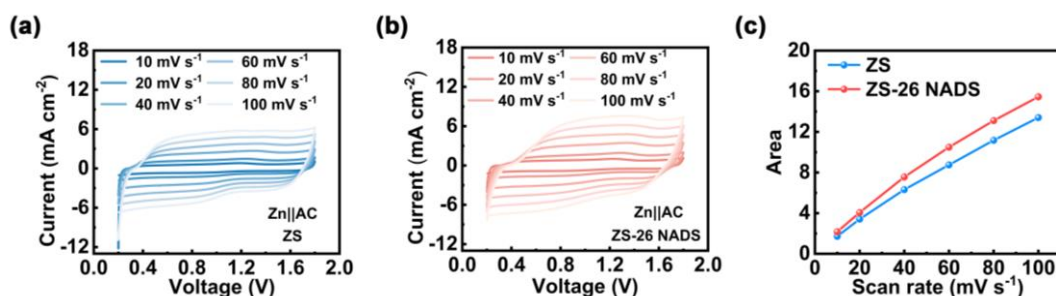


Fig. S35. The different scan rates of the CV of capacitors in (a) ZS and (b) ZS-26 NADS electrolyte. (c) The area of CV of capacitors in different electrolytes at various scan rates.

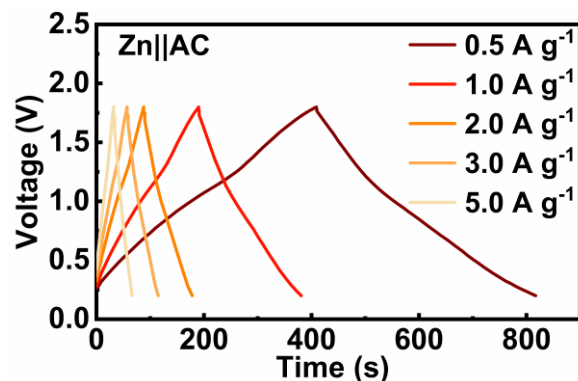


Fig. S36. The Galvanostatic charge/discharge curves (GCD) of Zn||AC capacitor in the ZS-26 NADS electrolyte.

Video

Video S1 Operando optical video of Zn anodes observed in symmetric cells with different electrolytes.

Reference

- S1 J. Hafner, *J. Comput. Chem.*, 2008, **29**, 2044-2078.
- S2 G. Kresse and J. Hafner, *Phys. Rev. B*, 1993, **48**, 13115-13118.
- S3 J. Perdew, K. Burke and Y. Wang, *Phys. Rev. B*, 1996, **54**, 16533-16539.
- S4 S. Grimme, *J. Comput. Chem.*, 2006, **27**, 1787-1799.
- S5 P. J. Stephens, F. J. Devlin, C. F. Chabalowski and M. J. Frisch, *J. Chem. Phys.*, 1994, **98**, 11623-11627.
- S6 S. Grimme, J. Antony, S. Ehrlich and H. Krieg, *J. Chem. Phys.*, 2010, **132**, 154104.
- S7 F. Weigend and R. Ahlrichs, *Phys. Chem. Chem. Phys.*, 2005, **7**, 3297.
- S8 T. Lu and F. Chen, *J. Comput. Chem.*, 2012, **33**, 580-592.
- S9 D. Spoel, E. Lindahl, B. Hess, G. Groenhof, A. Mark and H. Berendsen, *J. Comput. Chem.*, 2005, **26**, 1701-1718.
- S10 M. Abraham, T. Murtola, R. Schulz, S. Páll, J. Smith, B. Hess and E. Lindahl, *SoftwareX*. 2015, **1-2**, 19-25.
- S11 H. Berendsen, D. Spoel and R. Drunen, *Comp. Phys. Comm.*, 1995, **91**, 43-56.